2.8 Time-Resolved X-ray Techniques Development

The SRI-CAT time-resolved techniques program is part of the activities of the x-ray physics group and is primarily based on the sector 1 beamlines. This program has a diverse range of activities with the common

theme of measuring temporally evolving phenomena with x-rays. A major goal of this program is to develop instrumentation that can be used by other CATs at the APS. The best example of this is the beam choppers described below, which are now primarily used in non-SRI-CAT experiments. With G. Mourou, Z. Chang, D. Umstadter (all University of Michigan), and L. Young (ANL), we also co-organized a "Workshop on the Marriage of High Intensity Lasers with Synchrotrons" to explore the field of laser-pumped, x-ray probed techniques. Other efforts center on technique development to develop new experimental methods for both the ID and bending magnet beamlines. The fuel spray studies are an example of experiments that are conceptually straight-forward but require sophisticated use of equipment (fast detectors, special injector systems) to actually execute. Several aspects of the time-resolved efforts are integrated into other sector 1 programs. One of these, the measurement of transient behavior in materials using powder diffraction, is closely coupled with the high-energy x-ray program and is described in that section.

Future efforts of the time-resolved program will fall into two categories: studies that utilize the pulsed nature of the storage ring and those that do not. In the first case, development of a fast x-ray streak camera will allow the growth of techniques, such as image-correlation spectroscopy for pump-probe experiments. For the second case, emphasis will be given to continued study of transient material behavior. In many cases, these projects will be strongly coupled to the high-energy or sector 1 optics programs.

2.8.1 Fuel Spray Studies

Detailed analysis of the fuel spray process has been recognized as an important step in the overall aim of increasing combustion efficiency and reducing emission of pollutants, particularly for diesel engines. This has spurred considerable activity in the development of both optical and nonoptical techniques for measurements in diesel fuel injection systems. Despite significant advances in laser diagnostics over the last 20 years, the region close to the nozzle has remained impenetrable to experiments designed to acquire quantitative information due to multiple scattering by the large number and high density of droplets in the region. While other researchers are looking into the possibility of using lasers of ultrahigh power and ultrashort pulse to study this region, we report here the development of a new nonintrusive and quantitative technique to characterize the dense part of the fuel spray using monochromatic x-ray absorption techniques. X-rays are highly penetrative in materials composed of extremely dense droplets made of low-Z materials, which makes x-rays an excellent tool for fuel spray studies. We have developed the technique, using x-ray absorption of monochromatic radiation, to quantitatively determine the fuel density distribution in this optically impenetrable region with a time resolution better than one microsecond. The current quantitative measurements constitute the most detailed near-nozzle study of a fuel spray to date.

The fuel spray was generated using a high-pressure injector typical of that found in a passenger car. The diesel fuel used in the test was doped with a cerium-containing additive in order to increase its x-ray

absorption. Injection was performed into a spray chamber filled with inert gas at atmospheric pressure and at room temperature. SF_6, a very heavy gas, was used to create a relatively dense ambient environment in the injection chamber. The experiments were performed at the 1-BM beamline. A 5.989 keV x-ray beam was focused and then collimated by a pair of slits to a size of 500 μm (horizontal) × 50 μm (vertical). The transient x-ray attenuation signal due to the fuel spray was measured by an avalanche photodiode (APD). The APD response was proportional to the beam intensity over the range used in our experiment and was recorded every 2 ns by a digitizing oscilloscope. Since the APD is a point detector, the injection chamber was translated vertically and horizontally with respect to the x-ray beam, allowing the beam to probe various positions within the spray plume. The x-ray absorption technique using a monochromatic beam is distinguished from conventional measurements by the quantitative nature of the measurement. With proper calibration, the x-ray absorption directly yields the absolute fuel mass quantity in the beam and the mass distribution. In addition, anomalous absorption was measured above and below the Ce L_3 edge at 5.723 keV to confirm this calibration.

A plot of the time-dependent x-ray transmission 1 mm and 6 mm from the nozzle on the spray axis is shown in Fig. 2.89. For the data taken at 1 mm from the nozzle, the spray clearly arrives and leaves the beam at t = 0.11 and 0.5 ms, respectively. The leading edge of the fuel spray appears very abruptly, indicating a very distinct boundary between ambient gas

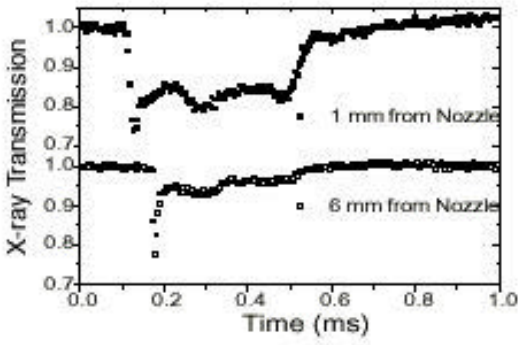

Fig. 2.89. Time evolution of the x-ray transmission on the spray axis 1 mm (solid square) and 6 mm (open square) from the nozzle.

and fuel spray with a compressed layer after the sharp edge. At 6 mm from the nozzle on the spray axis, the front edge of the spray arrives at the measuring point at a later time (0.19 ms).

The delay can be used to calculate the speed of the front edge. The absorption of the body of the spray decreased significantly, indicating a much lower fuel volume fraction there.

Based on the transmission values and the mass calibration, the amount of fuel in the path of the beam can be determined in a time-resolved manner. The normalized density (volume fraction of fuel) distribution is plotted in Fig. 2.90 for the leading edge of the spray (upper panel) and the main body of the spray (lower panel) at distances of 1 and 6 mm from the nozzle, respectively. The most striking feature of the plots in Fig. 2.90 is that the density of the fuel spray was significantly less than that of the bulk liquid fuel, even as close as 1 mm from the nozzle. The main body of the spray, the region that has been termed the “intact liquid core,” is actually composed of a liquid/gas mixture.

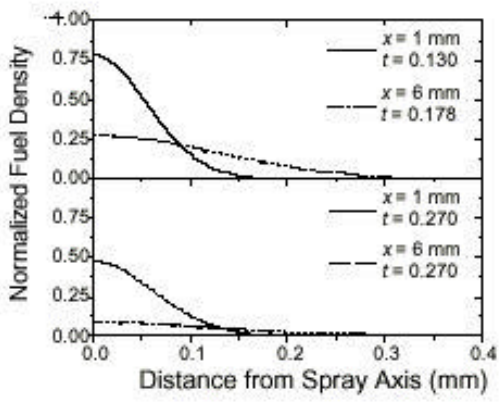

Fig. 2.90. Normalized radial distribution of the fuel density measured 1 and 6 mm from the nozzle at different instants in time (leading edge and main body of the spray intercepting the beam, respectively). A normalized density equal to unity implies the density of bulk liquid fuel (injection pressure: 500 bar; duration: 300 s).

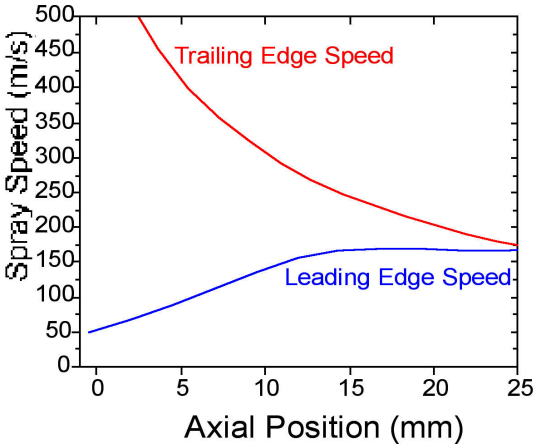

Fig. 2.91. Speed of the leading (blue line) and the trailing edge (red line) of the spray.

The speed of the leading edge has been determined in the experiment and is illustrated in Fig. 2.91. The speed increased slightly after the spray exited the nozzle, maintaining a nearly constant value that is slightly above the sonic speed in SF_6 (*ca* 140 m/s). Similarly, the speed of the trailing edge can also be derived. We note that initially the trailing edge traveled at a speed much higher than the sonic speed and gradually slowed to the value close to that for the leading edge. Thus far, the trailing-edge speed has never been determined by any other experiments. The trailing-edge speed provides invaluable information about the dynamics of the spray, such as generation of shock waves in the injection chamber.

In summary, by using monochromatic x-ray radiography, we have been able to study an optically much denser region of the spray than any study reported to date. The measurement is highly quantitative and time resolved. With further progress, a detailed spray structure of the near-nozzle region will be elucidated. These results are essential to the development of accurate theoretical models of fuel sprays and should lead to better nozzle designs. In addition, the synchrotron-based, time-resolved mono-chromatic x-ray radiographic technique has proven its usefulness not only in the field of spray science and technology but also in research areas dealing with transient phenomena of optically opaque materials, such as aerosols or heavy-element plasmas.

2.8.2 Polymer Thin-Film Dynamics and X-ray Damage

2.8.2.1 Polymer thin-film dynamics

On liquid surfaces, thermal excitations induce capillary waves with a long wavelength cutoff due to gravitation. The power spectrum associated with capillary waves can be expressed as $S(k) = (k_B T/\gamma)(k^2 + k_c^2)^{-1}$, where the cutoff is $k_c = \sqrt{\rho g/\gamma}$ (1 to 10 cm^{-1}), and ρ and γ are the liquid density and its surface tension,

respectively, and g is the gravitation. Theoretically, on liquid thin-film surfaces, the cutoff is simply modified by substituting g with $g_{eff} = g + F/(\rho d)$, where F is the effective interaction force per unit area (e.g., van der Waals forces) and d the thickness of the film. For $d < 1$ μm, $g_{eff} >> g$, resulting in a much larger cutoff k_c than that for bulk liquid surfaces. Such interaction prevents the long-range correlation that a free liquid surface possesses while essentially not affecting the short wavelength fluctuations. The shift of k_c to larger values can be visualized by x-ray diffuse scattering measurements, a well-suited technique for obtaining quantitative information about such thermal excitations.

Whereas bulk liquids have been investigated extensively, there are only a handful of quantitative investigations on liquid thin films, mainly due to difficulties in preparing samples with well-controlled film thickness and interfacial environment. Recently, we have attempted to study the surface behaviors of ultrathin polymer films for elucidating the capillary-wave properties on liquid thin-film surfaces and for investigating the substrate effects on these properties. True liquid-like behavior has never been observed even if the polymer-film thicknesses were much larger than the radius of gyration (R_G) and the polymer glass transition temperature (T_g). In this report, the surfaces of molten poly(tert-butyl acrylate) (PTBA) thin films on a silicon substrate have been investigated by specular and diffuse x-ray scattering.

In the experiments, we demonstrated that the surface of the polymer thin films exhibits modified capillary wave fluctuation, possibly due to the attracting van der Waals interaction between the substrates and the thin films (see Fig. 2.92). The observed capillary wave scattering is strongly dependent on the thin-film thickness. When the film thickness is close to or only a few times larger than R_G, the low-frequency cutoff of the wave-vector transfer along the surface (q_x) shifts to higher frequencies as the film thickness decreases. A signature of free liquid capillary scattering is a change of the exponent in the diffuse-scattering power law as a function of momentum transfer normal to the surface, q_z. This change was clearly observed for thicker films (Fig. 2.93).

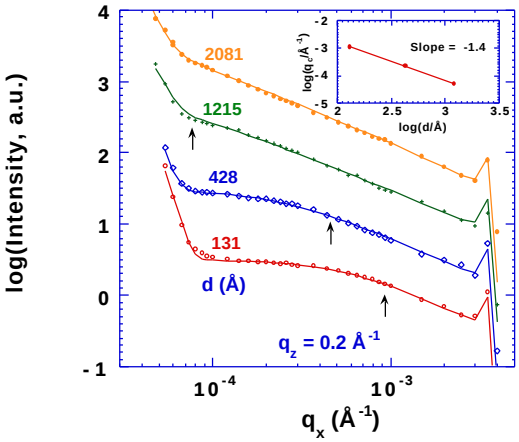

Fig. 2.92. Transverse diffuse scattering scans for the samples with various thicknesses (d) at q_z = 0.2 Å^{-1}. The fits to the data using modified capillary wave scattering theory (incorporating thin film effects) are shown as lines. The arrows indicate the cutoff locations. The inset depicts log(k_c) vs. log(d).

2.8.2.2 X-ray damage in polymer thin films

Despite the obvious occurrence of synchrotron x-ray damage to organic thin films, few attempts have been made to

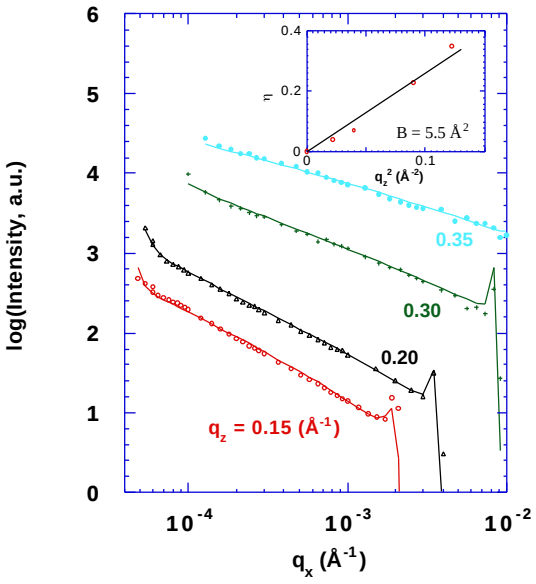

Fig. 2.93. Transverse diffuse scans from the sample with d = 2018 Å. The fits to the data using capillary wave scattering theory are shown as lines.

qualitatively determine their *morphological* changes during x-ray exposure. Frydman et al. (1997) used x-ray photoelectron spectroscopy and Fourier-transform infrared spectroscopy to study several different self-assembled monolayers (SAMs) on varying substrates. They found that the majority of the damage seems to occur at the surface of the film (especially if labile groups are present) rather than by removal of large amounts of film material. Despite the obvious surface changes, atomic force microscopy (AFM) pictures did not show any large scale increase in surface roughness but rather indicated the formation of "diamond-like" carbonaceous material with only a modest (< 4 Å) surface roughness.

We have used x-ray reflectivity at the 1-BM beamline to study x-ray damage of a polymer thin film. Reflectivity probes the electron-density profile of a film perpendicular to the surface and therefore allows us to obtain some of the important structural parameters necessary to quantify x-ray damage (such as the interfacial morphology), which cannot be obtained from spectroscopic techniques. The results indicate that most of the damage leading to a change in the reflectivity occurs at or near the film interfaces that are furthest apart. This can be deduced by the obvious disappearance of the oscillations during x-irradiation (Fig. 2.94) and by examining the surface roughness as a function of time (Fig. 2.95). We will perform further experiments, using both x-ray reflectivity and AFM, to further elucidate this important process. Especially of interest is whether AFM images will also show a pronounced increase in the top surface roughness.

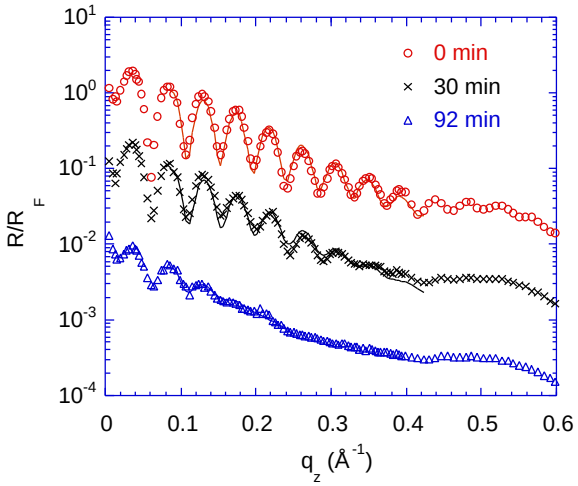

Fig. 2.94. Normalized reflectivity curves after three exposure times, including the two-layer fits. Curves are displaced for clarity.

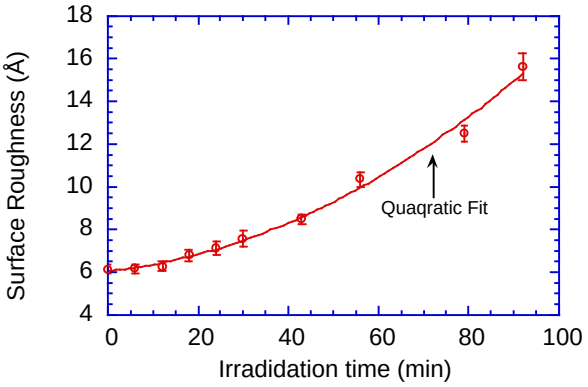

Fig. 2.95. The film-air interface width as a function of exposure time.

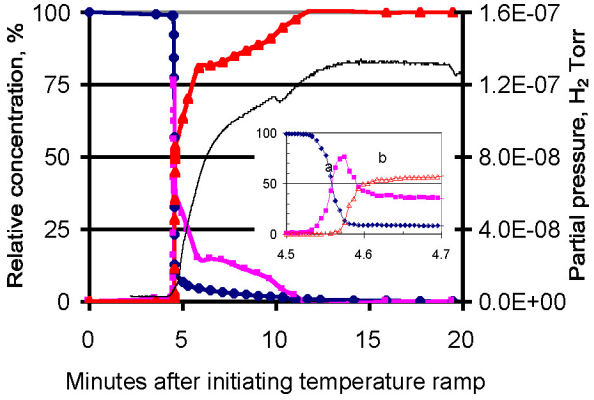

Fig. 2.96. Changes in the relative concentrations of different copper oxidation states in a $CuO/ZnO/Al_2O_3$ catalyst during reaction with a feed containing P_{O2}=6.9kPa, ramp rate = 2°C/min. Insert shows magnified area from 4.5 to 4.7 minutes after initiation of the temperature ramp, (♦) Cu^{+2}, (■) Cu^{+1}, (▲) Cu^0.

2.8.3 Time-Resolved X-ray Absorption Near-Edge Spectroscopy (XANES)

Pollution regulations for automobiles have become increasingly stringent during the past several years. Attempts to curtail emissions, while maintaining the efficiency of the internal combustion have resulted in substantial improvements. For further progress, however, alternatives to the internal combustion engine are being examined. One such alternative is the polymer-electrolyte membrane fuel cell, (PEM-FC). In a PEM-FC, H_2 is catalytically oxidized to water with the generation of electrical potential. In order to supply H_2 continuously to the fuel cell, a second catalytic process incorporating the partial oxidation of methanol, is used. Currently the catalyst used for this process is an industrial $CuO/ZnO/Al_2O_3$.

With a group from Northwestern University, we employed the dispersive-crystal mono-chromator (on 1-BM) for time-resolved XANES to obtain the *in situ* information about the CuO/ZnO catalyst in the oxidative methanol reforming reaction. In Fig. 2.96, the relative concentrations of Cu oxidation states (Cu^0, Cu^{+1}, Cu^{+2}) and the H_2 content in the gas phase product were plotted. The data show clear evidence that H_2 production is only associated with metallic Cu.

2.8.4 X-ray Beam Chopper Development at SRI CAT

Beam chopper development has been part of the time-resolved program at SRI CAT. Some of the design parameters included: (a) open time windows spanning the range from seconds to picoseconds; (b) fast rise and fall time for the transmitted pulse; and (c) a slow duty cycle relative to the open time of the beam chopper. In order to facilitate the large range of open time windows, three classes of beam choppers have been developed to make use of the temporal structure of the APS storage ring.

The first type of beam chopper is a slow shutter using a double-solenoid design. It

treats the temporal structure of the storage ring as a continuous source and may have an open time window as long as a few milliseconds.

The basic design for the fast motion of the solenoid is to over-drive the solenoid with a high voltage—but only for a few milliseconds to prevent the coil from burning out. A high-voltage power supply capable of delivering several amps of current is connected to a fast high-voltage switch. The first arm of the shutter is in the normal closed position, while the second arm is in the normal open position. Setting the timing of the trigger of the high-voltage switch for the two arms adjusts the length of the open time window.

This beam chopper, shown in Fig. 2.97, was set up to protect a CCD camera used as a detector for a diesel fuel spray experiment on 1-BM. Its open time was set to 4 to 5 milliseconds. The rise and fall time of the open time window was about 400 microseconds. It was operated at 1.4 hertz. This beam chopper can be adjusted for other operating parameters. Its limits are an open time window of about 200 microseconds and a repetition rate of about 30 hertz.

The second type of beam chopper is illustrated in Fig. 2.98. It is a fast shutter with a fixed open time window. It may or may not make use of the temporal structure of the APS storage ring, depending upon the experiment and the fill pattern of the storage ring. This beam chopper is modeled after a commercial high-speed air-bearing laser scanner. Basically, it is a rotating aluminum disk with a slot through the diameter. A

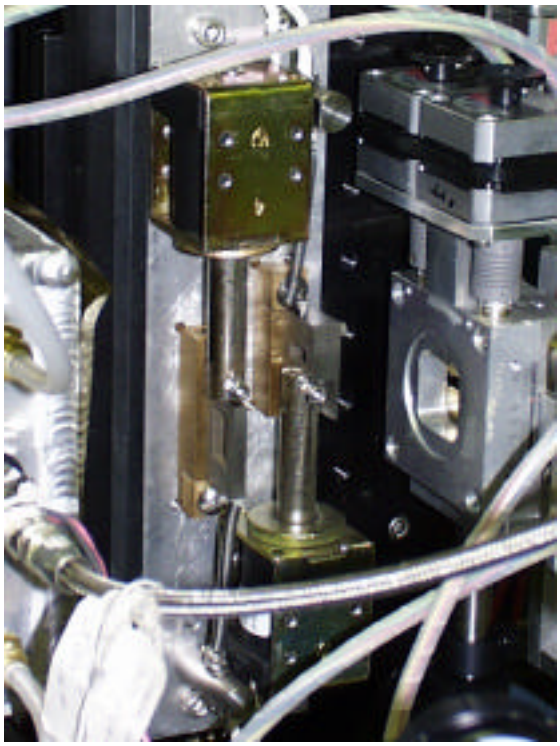

Fig. 2.97. Solenoid beam chopper.

nickel coating covers the circumference. Rotating at 1331 hertz, it has an open time window of about 2400 ns. There are two open window times per rotation of the disk. The dead time between open window times is 373 microseconds. A principal feature of this beam chopper is the high degree of rotational speed regulation of the disk. The uncertainty in the position of the transmission window (or jitter) is ± 3 ns at the 3-σ level (95% confidence level). Since the jitter is small relative to the open window time, the rotation of the beam chopper can be synchronized to the orbital frequency of the APS storage ring. This allows for the performance of time-resolved measurements. The time resolution is dictated by the experiment but may be as short as 50 ps when one filled “bucket” of the APS falls within the open time window.

If the temporal structure of the ring is not important, the beam chopper can be used to transmit a 2.4 microsecond pulse to map a time-resolved response. Carol Thompson and coworkers of Northern Illinois University have used this beam chopper to measure the time structure of the piezoresponse of a ferroelectric material at the 1-BM beamline and more recently at the BESSRC-CAT 12-ID beamline. The small size and portability of the beam chopper make it easy to transport and set up on other beamlines around the APS storage ring. This device is available to APS users upon request.

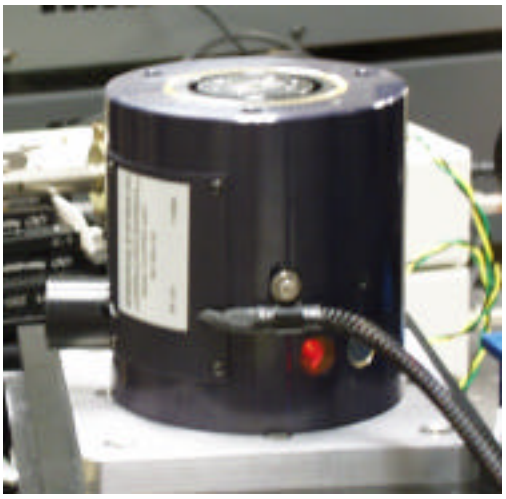

Fig. 2.98. High-speed beam chopper.

The third type of beam chopper is pictured in Fig. 2.99. It is an ultrafast shutter employing a rotating crystal mounted to the shaft of a precision high-speed motor. Using the small acceptance angle of perfect crystal reflections to produce an open window time as small as 12 ns, this beam chopper was designed to transmit only one filled bucket independent of the fill pattern of the APS storage ring. With the jitter in the time necessary to make one revolution less than 1 ns, the rotation of this beam chopper can be synchronized to the orbital frequency of the APS storage ring. Hence, it is possible to phase lock the rotation of the crystal to the temporal structure of the storage ring and work with only one selected bucket of the fill pattern.

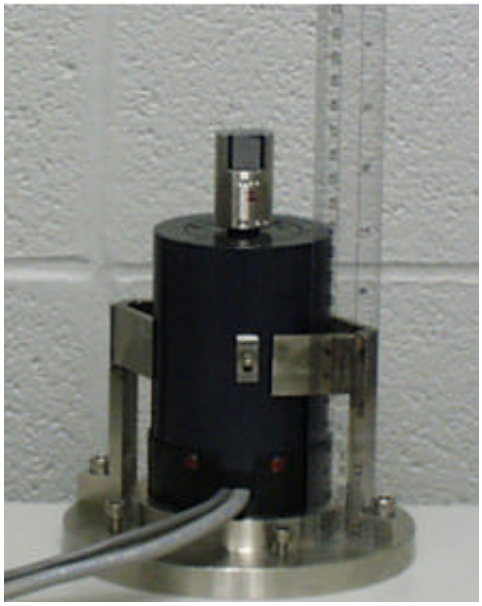

Fig. 2.99. Rotating crystal beam chopper.

The performance of this beam chopper has been tested at 1-BM, but it has not yet been used for experimental applications. It is also available to APS users upon request.